JMR EARLY CAREER SCHOLARS IN MATERIALS SCIENCE ANNUAL ISSUE: REVIEW

# Data-driven understanding of collective carbon nanotube growth by *in situ* characterization and nanoscale metrology

Mostafa Bedewy[a)]
*Department of Industrial Engineering, University of Pittsburgh, Pittsburgh, PA 15261, USA*

(Received 2 July 2016; accepted 14 November 2016)

Aligned carbon nanotubes (CNTs) possess great potential for transforming the fabrication of advanced interfacial materials for energy and mass transport as well as for structural composites. Realizing this potential, however, requires building a deeper understanding and exercising greater control on the atomic scale physicochemical processes underlying the bottom-up synthesis and self-organization of CNTs. Hence, *in situ* nanoscale metrology and characterization techniques were developed for interrogating CNTs as they grow, interact, and self-assemble. This article presents an overview of recent research on characterization of CNT growth by chemical vapor deposition (CVD), organized into three categories based on the growth stage, for which each technique provides information: (I) catalyst preparation and treatment, (II) catalytic activation and CNT nucleation, and (III) CNT growth and termination. Combining all three categories together provides insights into building the process–structure relationship, and paves the way for producing tailored CNT structures having desired properties for target applications.

Mostafa Bedewy

Dr. Mostafa Bedewy is an Assistant Professor at the University of Pittsburgh, where he leads the NanoProduct Lab (www.nanoproductlab.org). Before that, he worked as a Postdoctoral Associate at MIT in the area of bionanofabrication with Professor Karl K. Berggren. Also, he was previously a Postdoc at the MIT Laboratory for Manufacturing and Productivity (LMP), working with Professor A. John Hart on *in situ* characterization of carbon nanotube growth. In 2013, he completed his PhD at the University of Michigan in Ann Arbor, where he worked with Professor Hart on studying the population dynamics and the collective mechanochemical factors governing the growth and self-organization of filamentary nanostructures. He holds a Bachelor's degree (honors) in Mechanical Design and Production Engineering (2006) and a Master's degree in Mechanical Engineering (2009), both from Cairo University. Dr. Bedewy recently received the Robert A. Meyer Award from the American Carbon Society in 2016, the Richard and Eleanor Towner Prize for Distinguished Academic Achievement from the University of Michigan in 2014, and the Silver Award from the Materials Research Society (MRS) in 2013. His research interests include nanoscale manufacturing, metrology and material characterization, chemical vapor deposition, carbon nanotubes, self-assembly of hierarchical nanostructures, and engineering of biomolecular systems.

## I. INTRODUCTION

Aligned carbon nanotubes (CNT), referred to as CNT forests, have repeatedly been shown to possess great potential for transforming the fabrication of thermal interfaces, electrical interconnects, nanoporous membranes, and structural fibers/composites.[1,2] However, realizing this potential has proven to be challenging. A major challenge that hinders the successful integration of functional aligned CNTs into applications is the need for building the ***process–structure–property*** relationship that governs the fabrication of tailored CNTs by chemical vapor deposition (CVD). Here, what is referred to as "process" encompasses the catalyst preparation, catalytic activation, growth and deactivation steps of CNT growth by CVD. Importantly, CVD is a promising CNT fabrication method owing to its scalability, flexibility and the high quality of CVD-grown CNTs,[3,4] but a comprehensive understanding of the whole CVD process is still largely missing. The "structure" refers to the morphology of the individual CNTs, and their organization into the vertically aligned forest morphology, including their diameter distribution, number of walls, alignment, defects, deformation, and density. Finally, the "property" here focuses on the collective properties of the CNT forest structure as a whole, in contrast to the properties of individual CNTs.

Studying how the morphology evolves during the successive stages of CNT growth by CVD from substrate bound catalyst nanoparticles has shown that a typical CNT forest exhibits spatial variations of diameter,

Contributing Editor: Eric A. Stach
[a)]Address all correspondence to this author.
e-mail: mbedewy@pitt.edu, bedewygroup.com
DOI: 10.1557/jmr.2016.498

alignment, and density, as shown schematically in Fig. 1.[5–8] These variations arise from the dynamics of growth, which are dominated by time-varying kinetics of chemical decomposition, catalytic activation, catalyst poisoning/deactivation, and atomic diffusion.[9–16] Importantly, the non-uniform morphology of CNT forests influences their properties, such as in mechanical compression for example, which was shown to be affected by density gradients.[17] Hence, revealing the process–structure and structure–property relationships requires a comprehensive understanding of the atomic scale physicochemical processes underlying the bottom-up synthesis and self-organization of aligned CNTs. To that end, a large number of *in situ* nanoscale metrology and characterization techniques were explored over the past two decades for interrogating a large number of individual CNTs simultaneously as they grow, interact with each other, and self-assemble into the aligned morphology.

Many *model-based* efforts toward understanding CNT growth and termination have relied on one type of data such as the evolution of the forest height as a function of growth time for example, and used these kinetics to explain the behavior expected of a single CNT growing from a single catalyst nanoparticle. An inherent assumption in those studies is that the areal density of CNTs is uniform throughout the forest. However, *data-driven* approaches enabled by collecting more measurements of the spatiotemporal evolution of CNT morphology during growth revealed that a growing CNT forest behaves as a large population with a time-varying distribution of diameters, tortuosity, and density.[5,7,8] Moreover, the interactions among growing CNTs play an important role in creating the self-supporting aligned morphology, as well as in the eventual growth self-termination.[5,18]

In a typical CNT forest, billions of CNTs grow simultaneously per square centimeter and interact together as they collectively build the vertically aligned structure. As shown in Fig. 1, this collective growth process can be broken down to a number of successive stages that are herein lumped into three main categories: (I) *Catalyst preparation and treatment*, in which the seeding nanoparticles are created by a combination of thin film deposition and thermal/chemical treatment for dewetting into a population of nanoparticles; (II) *Catalytic activation and CNT nucleation*, in which the introduction of the hydrocarbon gas leads to catalytic surface reactions and the formation of arranged carbon atoms on the surface of the catalyst nanoparticles that form a cap, leading to the lift-off of a population of CNTs that interact together; and (III) *CNT growth and self-termination*, in which the growth proceeds after CNT crowding and self-organization until the density starts to decay leading to eventual growth self-termination.

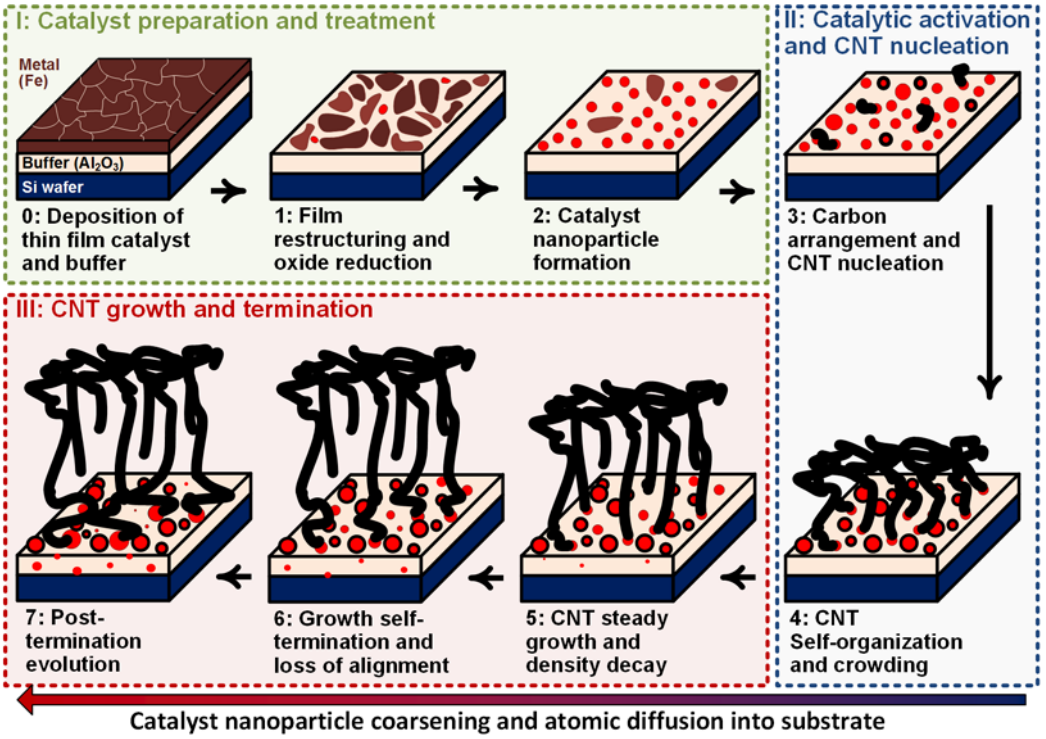


FIG. 1. Schematic showing the successive stages of the collective CNT growth mechanism, organized into three categories: (I) Catalyst preparation and treatment; (II) Catalytic activation and CNT nucleation; and (III) CNT growth and termination.

## II. CATALYST PREPARATION AND TREATMENT

In most cases catalyst nanoparticles for CNT forest growth are prepared by annealing a thin film deposited by a physical vapor deposition (PVD) technique such as sputtering or electron beam evaporation. Annealing the as-deposited film causes dewetting (also referred to as agglomeration), by which a population of nanoparticles are created by atomic surface diffusion at high temperature.[19] Although other methods of preparing the catalyst nanoparticles such as by optical and electron beam lithography,[20] colloidal self-assembly,[21,22] and block copolymer self-assembly[23] have been used to successfully grow CNTs, thin film dewetting remains the most common, owing to its simplicity, ease of integration with CNT processing, and its scalability.

A number of transition metal catalysts, and combinations thereof, were used to grow CNTs including Ni, Fe, Mo, Co, and others.[4,21,24–26] Also, a number of different materials were used as a buffer layer between the metal catalyst and the substrate (usually a Si wafer), such as Al, $Al_2O_3$, TiN, and $TiO_2$.[27] It was shown that the catalyst–substrate interactions dictated the chemical changes that the as-deposited iron catalyst undergoes on different buffers upon exposure to $C_2H_2$. In particular, high growth rate of small-diameter CNTs was observed from FeO on $Al_2O_3$ buffer, as opposed to the slow growth of large CNTs having thick walls on both TiN and $TiO_2$ buffers. Moreover, for the same buffer layer material aluminum oxide, different processing routes and film properties were shown to significantly influence CNT growth.[15] Over the years, many approaches were explored for modifying the catalyst to improve growth. For example, growth was prolonged by tuning the stoichiometry of bimetallic catalyst particles, such as Ni–Fe,[28] and Co–Mo.[29] In another study, the stability of the support (aluminum oxide) layer was improved by doping with Lanthanum (La),[30] which enabled growing CNT forests as high as 18 mm.[31] Recently, ion bombardment was used to modify the surface properties for CNT growth.[32]

It's noteworthy that the catalyst nanoparticle could act as a seed for CNT growth while remaining strongly bound to the substrate surface, in which case the growth is referred to as *base-growth*. On the other hand, if the catalyst nanoparticle is pushed upwards by the growing CNT, it is referred to as *tip-growth*, as has been shown for some Mo- and Co-containing catalysts.[33] In cases of strong interactions between the active catalyst nanoparticles and the underlying support layer, such as between iron and aluminum oxide, base-growth is the dominant mechanism.[15,34] Moreover, the growth mechanism was shown to shift between tip growth and base growth based on the diameter of the catalyst nanoparticle.[35] Previously, backscatter-electron imaging was used to show that there are no traces of metal nanoparticles on the top of grown CNT forests,[36] to confirm the base-growth process for Fe nanoparticle catalysts on aluminum oxide support layers. The rest of this article will focus on studying this catalyst system.

Film restructuring of the iron/aluminum oxide system was studied previously by a number of surface characterization techniques, such as scanning electron microscopy (SEM), atomic force microscopy (AFM), electron diffraction (ED), X-ray diffraction (XRD), X-ray photoelectron spectroscopy (XPS) and *in situ* grazing incidence small angle X-ray scattering (GI-SAXS).[7,15,27,37–43] Many imaging and chemical characterization techniques such as electron microscopy and XPS are typically difficult to employ *in situ* owing to the stringent requirements of low pressure, and limitations on the gases that can be introduced into the measurement chamber. On the other hand, scattering-based methods such as GI-XRD and GI-SAXS provided unique information on the morphology and chemical state of the catalyst during the preparation steps at higher pressures.

Environmental transmission electron microscopy (E-TEM) was recently used, as shown in Fig. 2, for the real-time observation of the collective process of catalyst nanoparticle preparation, CNT nucleation and eventual catalytic deactivation on thin TEM membranes. Electron diffraction (ED) enabled studying the structural and associated chemical changes as iron oxide reduces in the $H_2$ environment. Finally, real-time TEM imaging also enabled monitoring the evolution of a population of nanoparticles during annealing. Results revealed the progressive restructuring and reduction of the as-deposited iron oxide film that occur during annealing in $H_2$. As shown in Figs. 2(b)–2(e), the ED patterns before annealing exhibited multiple continuous rings, indicating diffraction from multiple crystalline structures that represent a mixture of oxide phases. As temperature is raised during annealing up to 750 °C, distinct reflection points on the rings emerge, which signifies the restructuring of a polycrystalline film to form larger crystallites. Even with dwelling at 750 °C for more than 100 min, the oxide reduction is not complete, as can be inferred from the presence of a mixture of rings corresponding to metallic Fe and oxide phases [Fig. 2(e)].

Hence, annealing the thin film iron oxide up to 750 °C in $H_2$ in vacuum (40 mTorr) does not fully reduce the catalyst to the metallic phase.[42,44] Experimental studies have also shown that heating using a hot tungsten filament up to 2000 °C produces atomic hydrogen that rapidly reduces the catalyst.[16,45] Other strong reducing agents such as ammonia ($NH_3$)[42] and hydrazine ($N_2H_4$)[46] were also shown to cause the complete reduction of iron oxide. The reduction and phase change of Fe catalyst are therefore dependent on the annealing conditions, such as temperature, pressure, dwell time, and the gas environment.

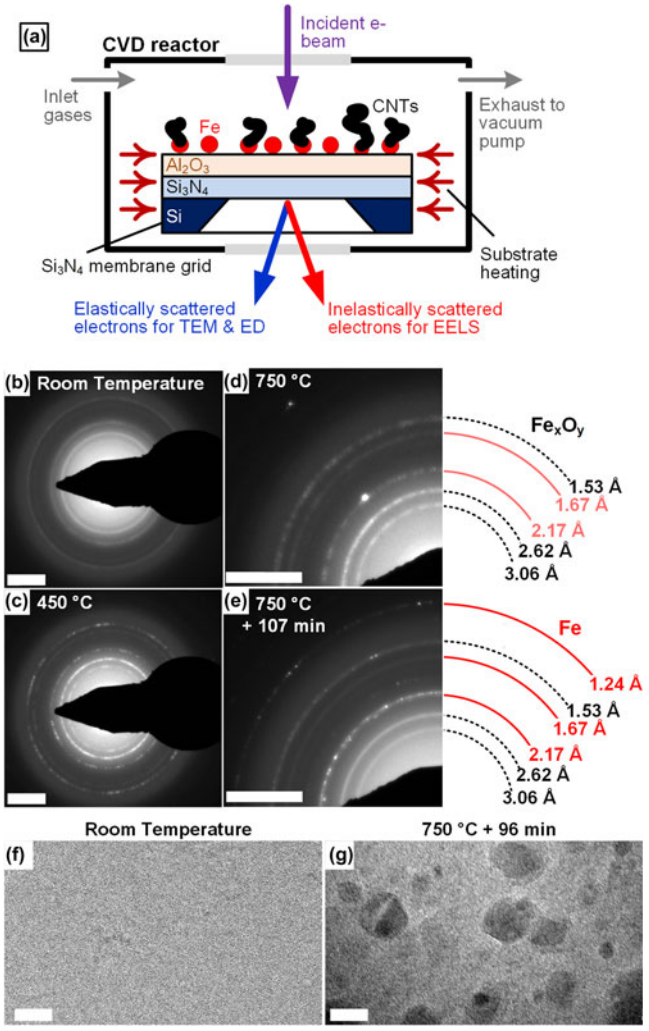


FIG. 2. *In situ* characterization of catalyst film evolution during annealing by TEM and ED. (a) Schematic showing the growth of CNTs on TEM membranes inside an E-TEM. (b–e) ED patterns during heating the $Fe_xO_y/Al_xO_y$ catalyst film in hydrogen, showing the reduction to metallic Fe with extended dwell time at 750 °C, as confirmed by the emergence of the red rings at interplanar spacings that are characteristic of metallic Fe (scale bar: 3 $nm^{-1}$). (f, g) TEM images taken at different temperatures, showing film restructuring during annealing and particle formation by dewetting after 96 min at 750 °C (scale bar: 10 nm). Adapted with permission from Ref. 43. Copyright 2016 American Chemical Society.

As shown in Fig. 3, *in situ* GI-SAXS was used to study the dynamics of nanoparticle formation by dewetting (agglomeration), and the results showed that this process is rapid once a sufficiently high temperature is reached during fast heating. Mounting the reactor in the beamline of a synchrotron source also enabled GI-SAXS to uniquely track the time evolution of the statistical distribution of nanoparticle sizes and shapes.[38] Although GI-SAXS is well-suited to studying dewetting, once CNTs start nucleating it becomes difficult to decouple the scattering coming from CNTs form that coming from the nanoparticles. Eventually, CNT scattering dominates, obscuring any information about the evolution of nanoparticles during growth. Importantly, using scattering intensity as an indication of CNT, both GI-SAXS and GI-XRD clearly demonstrate that the lift-off of aligned CNT forests from tangled CNT mats is an abrupt process.[38,47]

## III. CATALYTIC ACTIVATION AND CNT NUCLEATION

Although, there are different schools of thought with respect to the exact atomic scale physicochemical processes underlying catalytic activation and nucleation of CNTs,[48] the process generally proceeds by the arrangement of carbon atoms on the surface of the catalyst nanoparticles, leading to cap formation and liftoff. A major challenge is identifying which phase is the catalytically active phase and which pathways leads to the most active CNT growth (faster growth kinetics and higher density of CNTs). Toward this end, Hofmann et al. used *in situ* XPS to demonstrate that reducing $Fe^{3+}$ and $Fe^{2+}$ to the more catalytically active metallic Fe phase is required for efficient CNT nucleation.[42] De los Arcos et al. also used the same characterization technique of *in situ* XPS, as shown in Fig. 4, to identify that active catalyst phase to be either Fe or FeO depending on properties of the buffer layer (chemical and morphological).[39] An advantage of using XPS is that it enabled directly monitoring that the transition from chemisorbed carbon to graphitic carbon deposition by looking at the evolution of the core carbon 1*s* peak. This transition of binding energy, shown in Fig. 5, can be used as an indication of the formation and lift-off of nucleating CNTs.[41] However, the penetration depth in XPS analysis is typically limited (~2 nm), which prevents the continued characterization once CNTs cover the catalyst nanoparticles.

The catalytic activity and phase dynamics of Fe-based catalysts were also studied by *in situ* ED, and results showed that iron carbide is formed as a result of exposing body-centered cubic (BCC) metallic iron to $C_2H_2$. In that study, the cementite phase ($Fe_3C$) was shown to be the active phase required for CNT growth, and the carbon-rich Hägg phase ($Fe_5C_2$) was shown to be the inactive (catalytically poisoned) phase.[49] Additional *in situ* GI-XRD characterization also showed the dynamics of catalyst phase change, wherein if you start with FCC-rich iron catalyst (γ-Fe), the metallic Fe is the active phase without the need for carbide formation. On the other hand, if you start with a BCC-rich metallic phase (α-Fe), carbide formation is important for the growth process.[50]

Hence, individual catalyst nanoparticles within large populations typically follow a variety of different pathways during the successive stages of annealing and

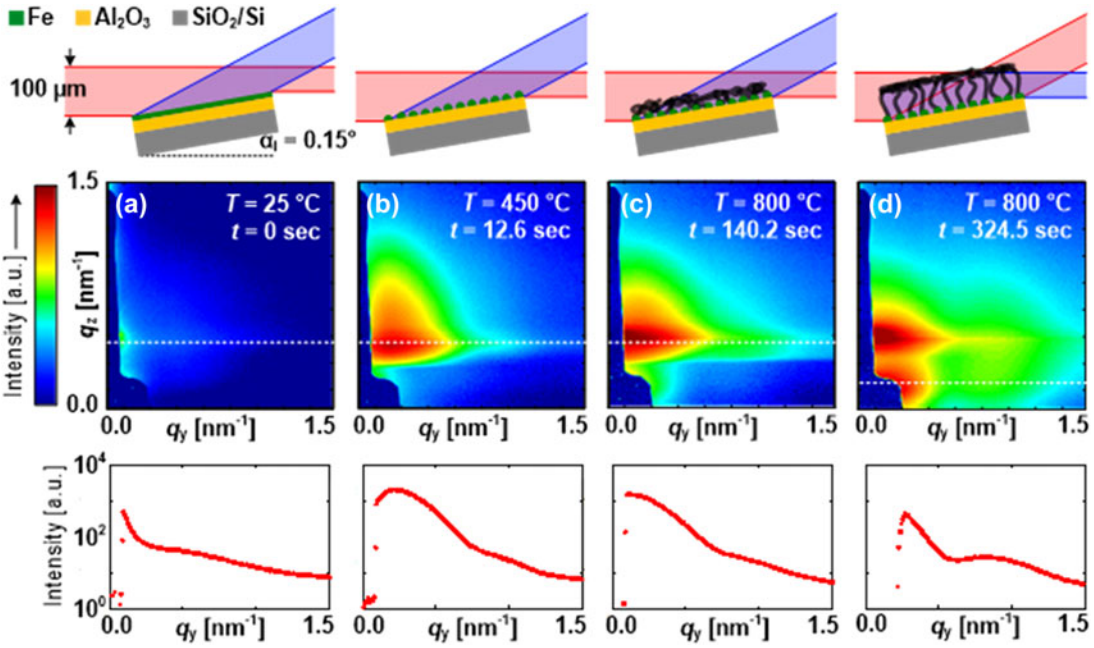


FIG. 3. Schematics and *in situ* GI-SAXS patterns of the successive stages of catalyst preparation and CNT nucleation: (a) As-deposited Fe/$Al_xO_y$ film before heating; (b) Fe/$Al_xO_y$ film being rapidly heated, showing the formation of nanoparticles by dewetting; (c) CNT nucleation from Fe catalyst nanoparticles; and (d) CNT growth, where scattering from CNTs from the transmitted X-ray beam dominate the collected 2D pattern, obscuring scattering from the nanoparticles. A schematic of scattering geometry corresponding to each pattern is shown above the pattern, and a plot of X-ray intensity ($I$) versus inverse space parameter ($q$) along the dashed line in the SAXS pattern is shown below each pattern. The blue shaded part of scattering is used for analysis. Reprinted with permission from Ref. 38. Copyright 2012 American Chemical Society.

changes in the gas environment. These observations highlight the importance of any inherent variability in size, shape, and chemical composition among catalyst nanoparticles. Also, the spatial distribution of surface contaminants and any other local interactions can play a role in influencing the catalytic activity and the phase change dynamics.

At the scale of individual nanoparticles, *in situ* E-TEM imaging of CNT nucleation informed the understanding of the atomic scale mechanisms of graphitic cap formation and liftoff.[41,50–53] Hence, E-TEM enabled the direct measurement of CNT growth kinetics of individual CNTs growing from a single catalyst nanoparticle, as shown in Fig. 6.

More recently, E-TEM has been applied to observe the nucleation and growth of a large number of CNTs within the field of view, as shown in Fig. 7. *In situ* E-TEM imaging of catalyst populations, with more than 200 particles in the same image enabled plotting the population kinetics of catalyst nanoparticle formation by dewetting [Fig. 7(e)]. The accelerated dewetting behavior upon $C_2H_2$ exposure observed in this study was attributed to the reduction of iron oxide, leading to the sudden appearance, or "popping," of the fully formed catalyst nanoparticle in view in the E-TEM image.[43] *In situ* TEM imaging also enabled studying the mechanical interactions between CNTs as they crowd each other and self-organize into the aligned structure [Figs. 7(f) and 7(g)].[43,54]

Importantly, different carbon-containing feedstock gases were used in CVD growth of CNTs, including acetylene,[55] ethylene,[56] methane,[57] ethanol,[58] and carbon monoxide.[59] Moreover, other additives were explored to assist growth by either accelerating the growth rate or prolonging the catalyst life, such as water, oxygen, air, ethanol, carbon dioxide, acetone, tetrahydrofuran, methylbenzoate, and benzoaldehyde.[4,60–63] This review focuses on CVD growth of CNTs using acetylene and ethylene feedstock, and does not focus on the chemistry of growth enhancers.

## IV. CNT GROWTH AND TERMINATION

Toward a mechanistic understanding of CNT growth and termination, characterization of the structure of a CNT forest is needed: from the macroscopic dimensions down to the atomic scale structure. In contrast to the previous category, which relied heavily on surface characterization techniques, the third category involves noncontact sensing of CNT forests and imaging their hierarchical morphology at multiple length-scales, shown in Fig. 8, along with spectroscopic and scattering-based techniques. For example, the evolution of forest morphology was heavily studied using *ex situ* SEM, to reveal the mechanism of growth temination.[64,65]

A large number of *in situ* and *ex situ* techniques were previously explored for the nondestructive characterization of CNT growth kinetics. For example, optical photography

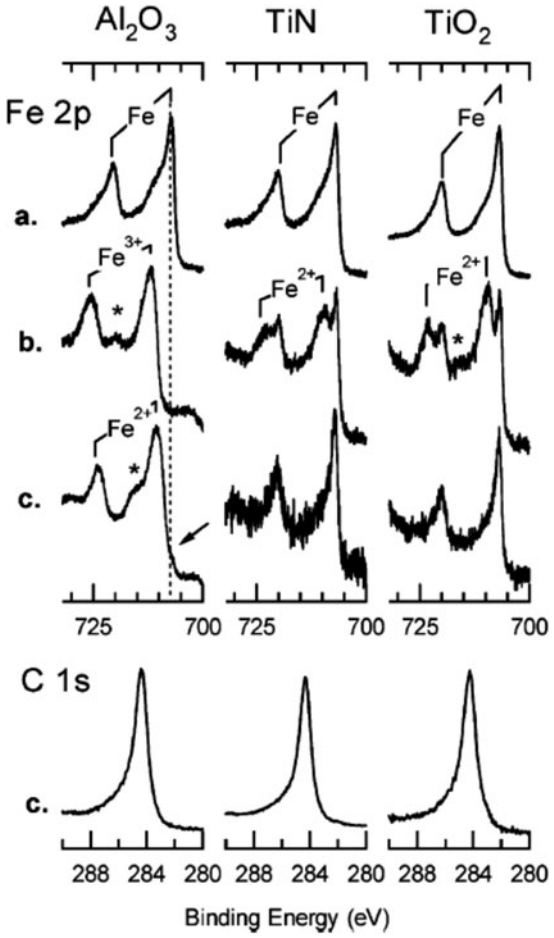


FIG. 4. *In situ* XPS results, showing the Fe 2*p* core lines at successive stages of catalyst preparation and CNT nucleation on different support layers ($Al_2O_3$, TiN and $TiO_2$). (a) Measurement collected before annealing (as-deposited). (b) Measurement collected after annealing in a vacuum ($10^{-5}$ mbar) up to 840 °C for 8 min. (c) Measurement collected after annealing the samples for 8 min followed by exposure to $C_2H_2$ for 5 s. Reprinted with permission from Ref. 39. Copyright 2004 American Chemical Society.

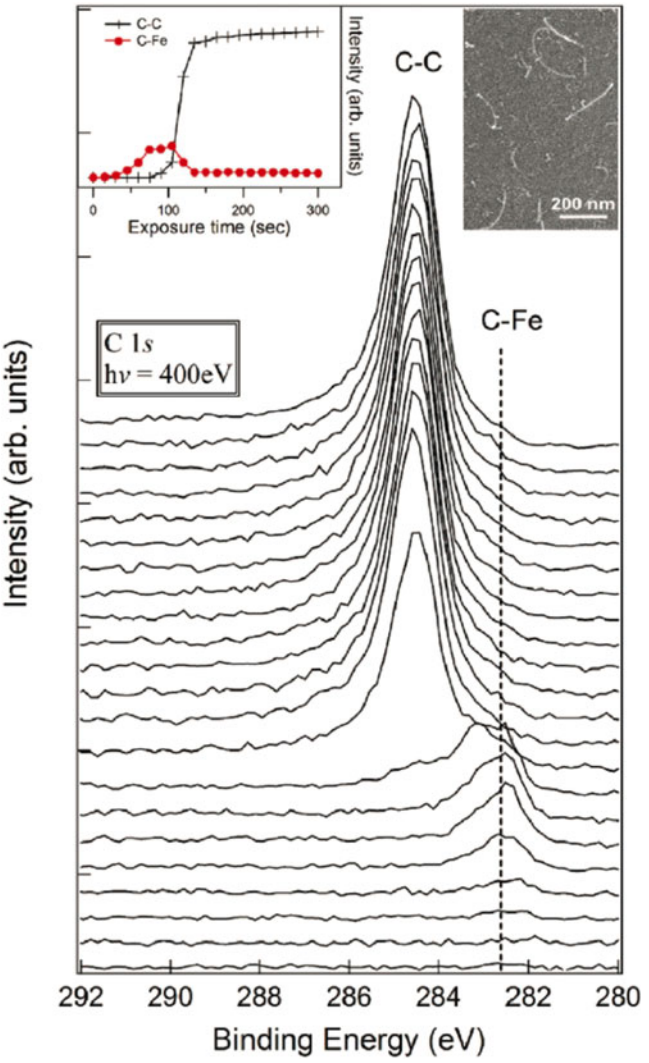


FIG. 5. *In situ* XPS of the C 1*s* core level during Fe exposure to $C_2H_2$ at 580 °C ($\sim 2 \times 10^{-7}$ mbar). Inset on the right show an SEM image of CNTs grown on the same part of the substrate. Inset on the left show the time-evolution of the chemisorbed (dots) and graphitic (crosses) carbon peaks. Adapted with permission from Ref. 41. Copyright 2007 American Chemical Society.

and videography,[67,68] optical interference,[69] single-slit laser diffractography,[70] time-resolved reflectivity,[9] laser triangulation,[71,72] and cycling of growth to create stacked structures visible by SEM.[64,73,74] Importantly, all of the abovementioned methods only enables quantifying the height kinetics. On the other hand, real-time mass measurements are more challenging, and have been achieved in the past generally by using a microbalance either *ex situ*,[5,75] or *in situ*.[76] Weighing samples, however, imposes limitations on the resolution of the measurement and does not enable spatial mapping of mass and density across an individual forest.

Indirect measurements of density were obtained from *ex situ* Z-contrast transmission electron microscopy (Z-STEM) imaging, as well as from real-time changes in the effective extinction coefficient in time-resolved optical reflectivity (TRR).[77–79] Also, *in situ* Raman spectroscopy can be used to provide a measure of relative mass kinetics from real-time integration of the area under the G-band.[80–83] Real-time monitoring of the G-band during growth of single-wall CNTs was instrumental in demonstrating that the growth rate is dependent on CNT chirality.[84] Recently, *in situ* electron energy loss spectroscopy (EELS) was used to quantify the accumulating carbon on the surface during CNT growth inside E-TEM, by plotting the time evolution of the carbon K-edge near-edge structure.[43] While some of these indirect approaches can be utilized for spatial mapping of density, they can only infer relative density.

As shown in Fig. 9, X-ray attenuation has been shown to enable accurate spatial mapping of absolute mass density of CNT forests down to a spatial resolution of 10 μm

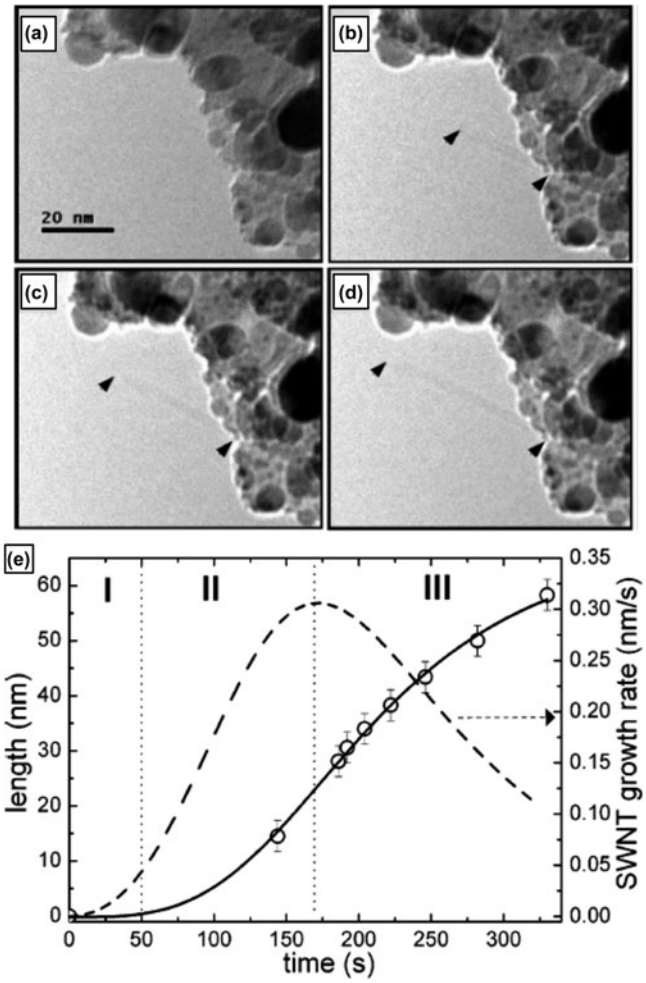


FIG. 6. (a–d) *In situ* TEM images showing the growth of a single CNT with time. (e) Extracted growth kinetics for an individual CNT. Adapted with permission from Ref. 51. Copyright 2006 American Chemical Society.

(limited by the size of the focused/trimmed synchrotron X-ray beam). A major advantage of this approach is that information about the evolution of diameter distribution and alignment are obtained simultaneously by analyzing SAXS patterns, as shown in Fig. 10.[5–7,72,85] In fact, Hermans orientation parameter can be used to measure the degree of alignment by quantifying the anisotropy in scattering patterns, obtained by either small angle neutron scattering (SANS)[86] or SAXS.[5,72,85] Combining high resolution spatial mapping of X-ray scattering and intensity attenuation measurements,[5,7] with real-time height kinetics of CNT growth obtained by noncontact laser triangulation,[71,72] enabled revealing the spatiotemporal evolution of mass density, number density, and cumulative CNT areal density with unprecedented accuracy throughout the stages of CNT growth [Fig. 9(b)].

As a result, CNT forest growth is explained as a time-varying population of individual CNTs that have a variation of growth rates, while interacting together

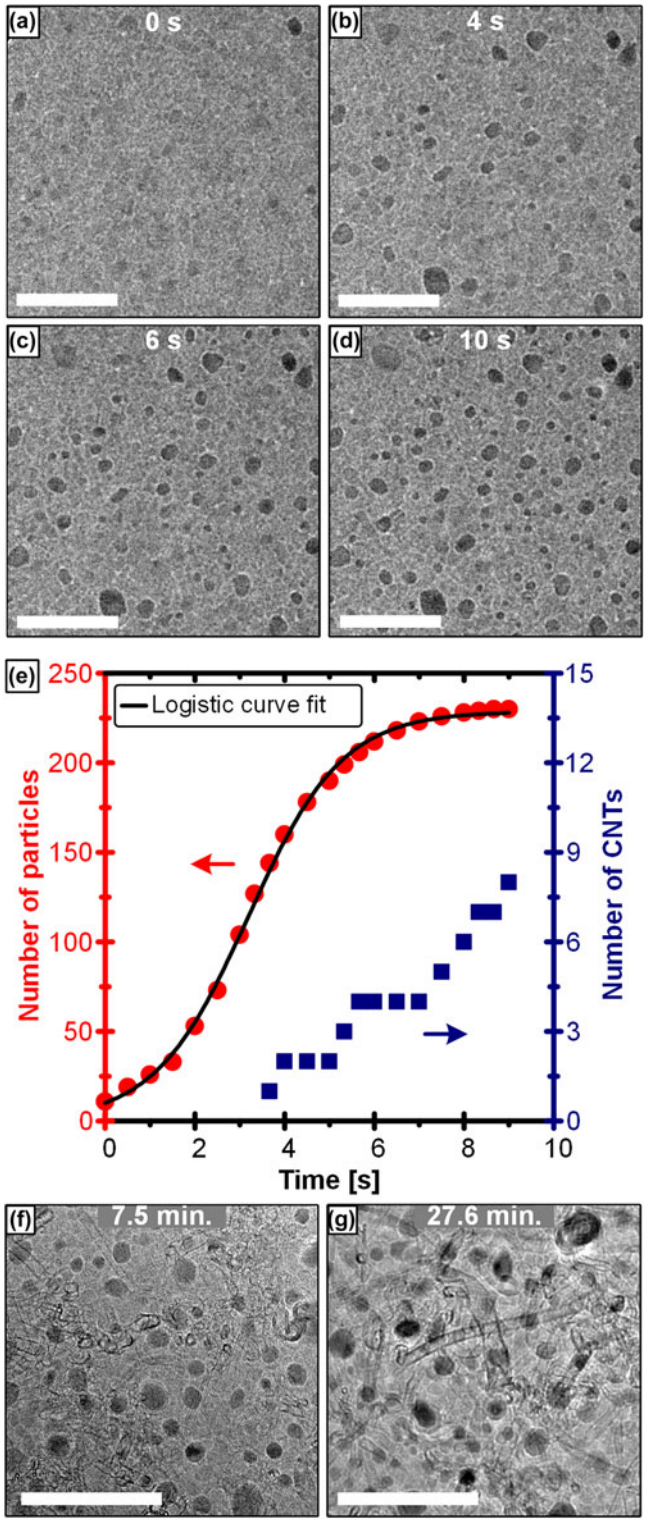


FIG. 7. (a–d) *In situ* E-TEM images showing the population dynamics of nanoparticle formation by dewetting as well as the nucleation of CNTs (Scale bar is 50 nm). (e) Time evolution of the number of nanoparticles and nucleating CNTs. (f, g) TEM images showing the mechanical interactions between CNTs and their self-organization during crowding (Scale bar is 50 nm). Adapted with permission from Ref. 43. Copyright 2016 American Chemical Society.

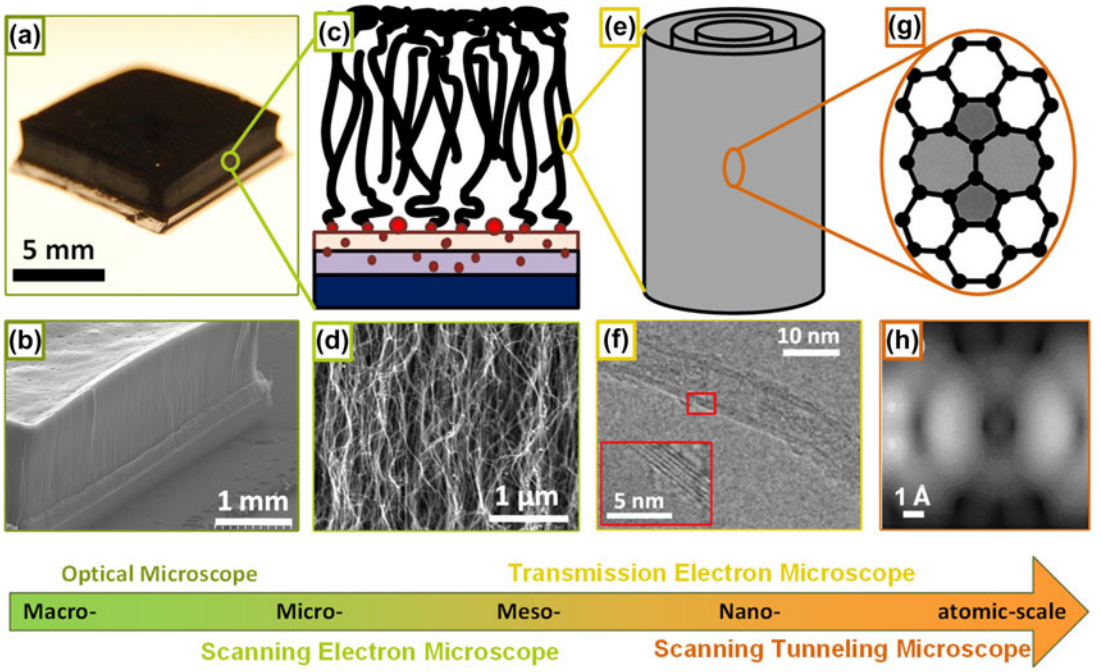


FIG. 8. Imaging a CNT forest at multiple length-scales. (a) Optical imaging of the macroscale forests (Adapted with permission from Ref. 7. Copyright 2011 American Chemical Society) (b) SEM imaging of the microstructure (Adapted with permission from Ref. 7. Copyright 2011 American Chemical Society). (c) Schematic of the nanoscale and mesoscale morphology of the tangled array of tortuous CNTs. (d) SEM showing the hierarchical forest morphology of bundled and tortuous CNTs (Adapted with permission from Ref. 7. Copyright 2011 American Chemical Society). (e) Schematic showing the concentric walls of a multi-wall CNT. (f) TEM image showing the walls of a CNT (Adapted with permission from Ref. 7. Copyright 2011 American Chemical Society). (g) Schematic showing the atomic structure of graphitic carbon walls with a Stone–Wales defect (Adapted with permission from Ref. 66. Copyright 2000 Elsevier). (h) STM image of CNT wall with Stone-Wales defect (Adapted with permission from Ref. 66. Copyright 2000 Elsevier).

within a growing forest. This collective growth picture emerged in contrast to studies that explain CNT forest growth behavior based on mathematical modeling of the behavior of a single catalyst nanoparticle-CNT system.[9,36,87,88] As shown in Fig. 9(b), the mass kinetics exhibit an S-shaped curve, which is fitted by the Gompertz model of population growth. This phenomenological fit indicated that the CNT population dynamics exhibit an autocatalytic nature. Combing this result with the evolution of diameter distributions during CNT growth [Fig. 10(b)] reveals the diameter dependent population growth dynamics [Fig. 10(c)]. Hence, small angle X-ray scattering (SAXS)[85,89] and ultra-small angle X-ray scattering (USAXS)[90] provide accurate information about density, diameters, bundle size, and alignment of CNTs in a growing forest.

Taken together, these results help paint a picture of the collective growth mechanism of CNT forests, as shown schematically in Fig. 1, starting with the nucleation of randomly oriented CNTs that interact with each other as their density increases. This crowding leads to the build-up of a self-supporting aligned morphology when the density reaches a threshold that was previously identified by numerical and experimental analysis to be in the order of $10^9$ CNTs/cm$^2$.[5,7] The CNT forest then grows steadily until density starts to decay as a result of the deactivation of individual CNTs in the growing population. This density decay proceeds until the density becomes too low to support the vertically aligned forest structure (lower than the abovementioned threshold density), at which point growth self-termination is observed. At the point of termination, forest height stops increasing, which is characterized by significant loss of alignment at the bottom of the forest.[5,7]

It is also probable that some CNTs continue to grow beyond the apparent cessation of forest height kinetics, but their number is too small to push the forest upward. This post-termination evolution likely leads to the accumulation of more tortuous CNTs at the interface between the forest and substrate, and may help control the adhesion of the as-grown CNT forest to the substrate on which it is grown. Hence, employing different cooling recipes, along with using $H_2O$ etching can tune forest–substrate interactions.[91]

## V. OUTLOOK ON REMAINING CHALLENGES

Based on the current understanding of CNT growth dynamics, there have been significant advances toward controlling CNT growth by CVD, such as efforts toward improving the control on CNT diameters, chirality, and/or density.[37,61,92–95] In the future, more improvements are

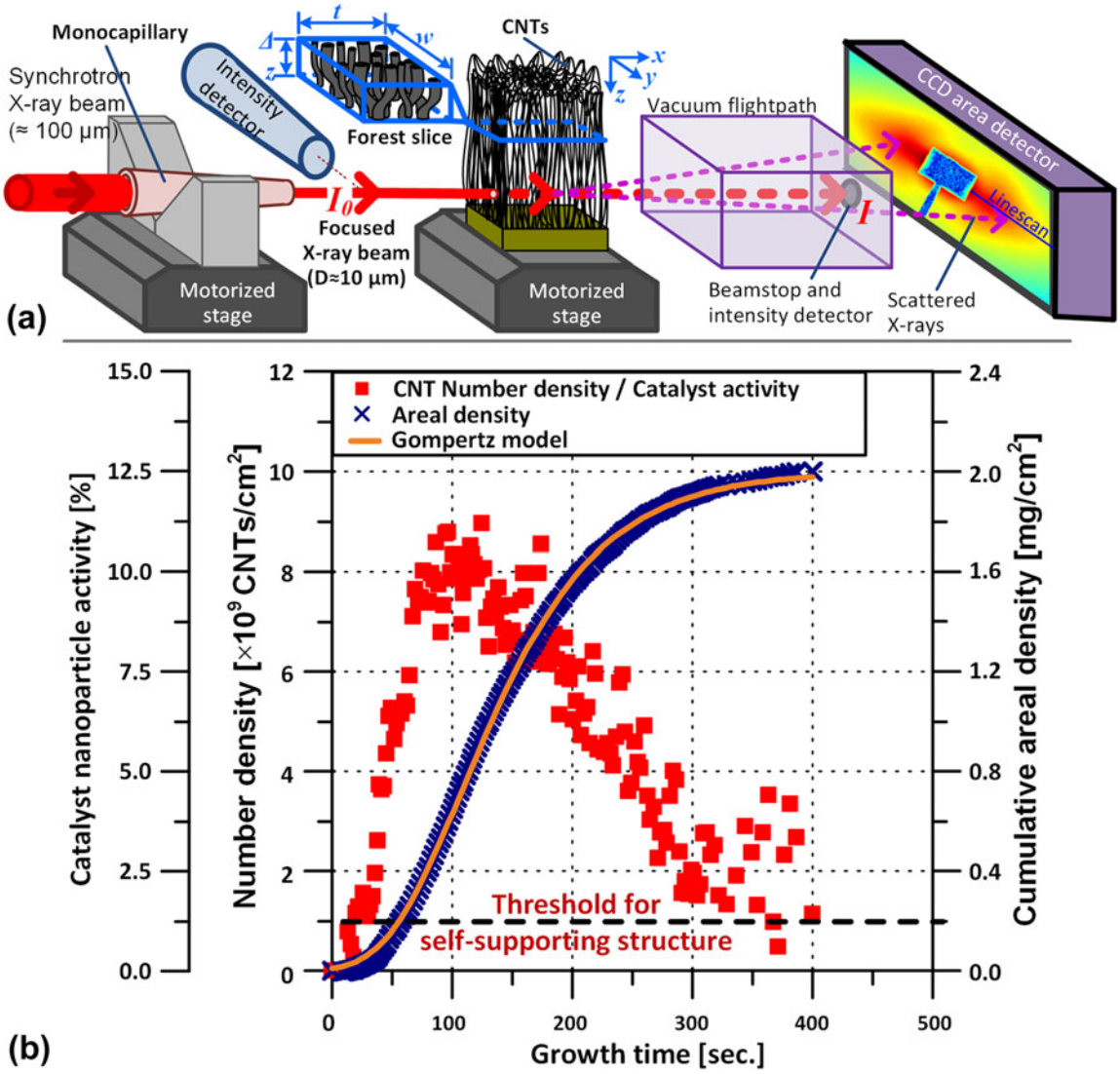


FIG. 9. (a) Schematic of the experimental set-up, wherein a CNT forest is placed on a motorized stage in a synchrotron beamline, and the beam is focused to a 10 μm spot. (b) Time evolution of mass density and number of density of CNTs, fitted to a Gompertz model of population growth. Adapted with permission from Ref. 7. Copyright 2011 American Chemical Society.

expected in the area of catalyst design and process engineering toward more deterministic control on the overall CNT quality (straightness and defect density) and precise atomic structure, including both mono-chiral and monodisperse diameter distribution of as-grown CNTs. In addition, more understanding on what factors determine whether a catalyst nanoparticle becomes active or inactive in a large population is likely to come by combining multiple *in situ* characterization techniques, such as combining TEM, ED, and EELS inside the E-TEM.[43] Understanding the spatial distribution of catalytic activity on substrates that arise from chemical coupling effects,[96] or from designed catalyst gradients/steps,[60,97] also enables engineering the three-dimensional geometry of microscale/macroscale CNT structures.

Another challenge that still plagues CNT growth is the deactivation of growth or self-termination, which was previously heavily studied, leading to proposing multiple mechanisms that are likely to be competing, such as catalyst poisoning, overcoating, evaporation or diffusion, nanoparticle coarsening and CNT mechanical coupling.[9,16,18,36,98–100] Studying the mechanochemical aspects of CNT growth, wherein the effects of mechanical forces on the catalytic process are analyzed both experimentally and numerically, is an area of current research and will enable better understating and control on the CNT growth process. A deeper understanding of all the competing deactivation mechanisms and identifying the dominant ones will open the door for approaches to overcome them. This is still required for the fabrication of

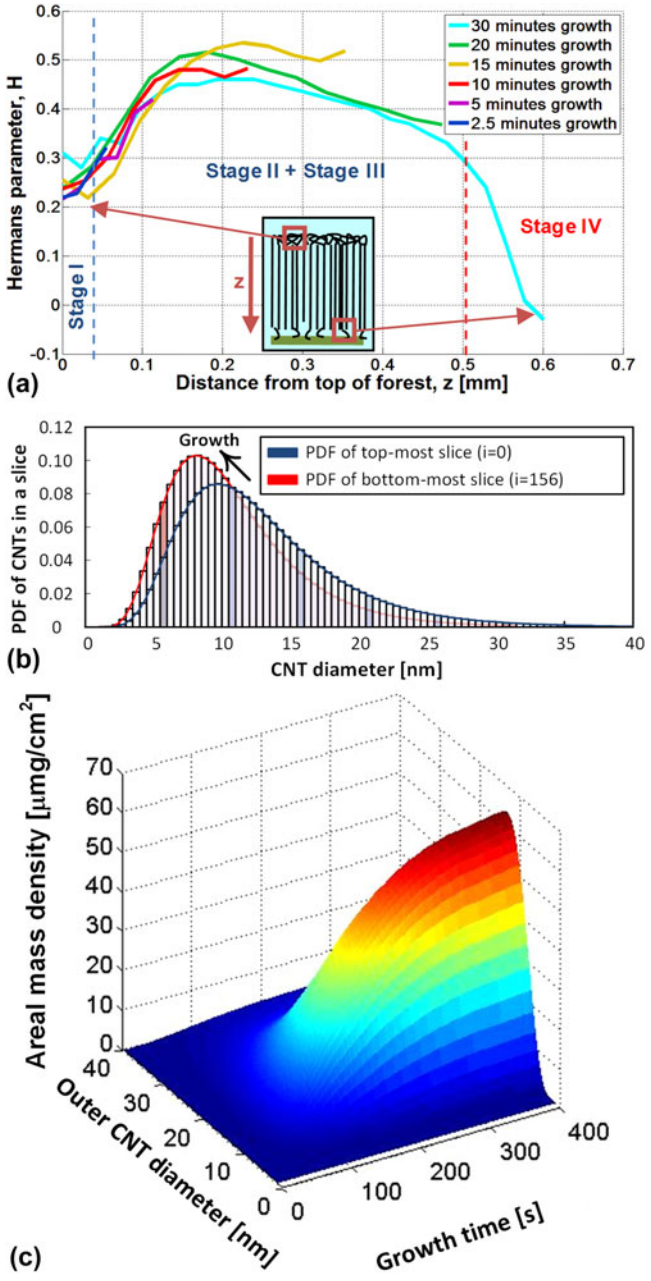


FIG. 10. (a) Spatial mapping of the Hermans orientation parameter by processing SAXS patterns for forests grown in a hot wall reactor for different growth times. Adapted with permission from Ref. 5. Copyright 2009 American Chemical Society. (b) Probability density function of CNT diameter distribution in the topmost and bottommost slices of a CNT forest. Adapted with permission from Ref. 8. Copyright 2012 Elsevier. (c) Diameter dependent growth kinetics obtained by combing diameter distributions with forest mass kinetics. Adapted with permission from Ref. 8. Copyright 2012 Elsevier.

ultra-long CNTs for application such as structural fibers and transmission lines.

Finally, from a practical perspective, the realization of many applications requires scaling the fabrication process, such as by roll-to-roll processing,[101] along with exercising more control on the inherent process variabilities that could compromise the properties of produced CNTs. Integrating aligned CNT films into functional devices invites the need to grow CNTs directly on different types of substrates such as metallic foils for instance.[22,102] Moreover, some applications require weak adhesion with substrate, such as in cases of transfer.[103] Other applications require strong adhesion, such as using CNTs as adhesives,[104] and rolling CNTs to form horizontally aligned structures.[91,105] Hence, controlling the post-termination evolution, shown in Fig. 1, could be an important complement to controlling CNT growth, to tune the mechanical adhesion, as well as the electrical and thermal resistance at the CNT-substrate interface.

## VI. CONCLUSIONS

This article presented a nonexhaustive overview of different characterization techniques that were utilized to study the successive stages of collective CNT forest growth, with particular focus on methods that are based on synchrotron X-ray scattering and mass attenuation, environmental transmission electron microscopy (E-TEM), electron diffraction (ED), and other spectroscopic techniques. *In situ* techniques were classified into three categories depending on the stage of the growth process. As shown schematically in Fig. 1, in the first category of catalyst preparation and treatment, thin film restructuring and nanoparticle formation by dewetting are characterized by surface characterization techniques during annealing. The second category of studying catalytic activation and CNT nucleation included efforts toward understanding the atomic pathways leading to the arrangement of carbon atoms on the catalyst and the lift-off of CNTs that interact with other CNTs in proximity. Finally, the third category summarized research on monitoring CNT growth and termination, with emphasis on methodologies for understanding the mechanochemical kinetics and mechanisms of catalytic deactivation. Combining all three categories together provides insights into building the process–structure relationship, which is at the heart of the science and technology of CNT fabrication. Hence, these efforts open the door for producing designed CNT structures having predictable morphology and tailored properties for specific applications.

## REFERENCES

1. R.H. Baughman, A.A. Zakhidov, and W.A. de Heer: Carbon nanotubes—The route toward applications. *Science* **297**(5582), 787 (2002).
2. M.F.L. De Volder, S.H. Tawfick, R.H. Baughman, and A.J. Hart: Carbon nanotubes: present and future commercial applications. *Science* **339**(6119), 535 (2013).
3. A.M. Cassell, J.A. Raymakers, J. Kong, and H. Dai: Large scale CVD synthesis of single-walled carbon nanotubes. *J. Phys. Chem. B* **103**(31), 6484 (1999).

4. K. Hata, D.N. Futaba, K. Mizuno, T. Namai, M. Yumura, and S. Iijima: Water-assisted highly efficient synthesis of impurity-free single-walled carbon nanotubes. *Science* **306**(5700), 1362 (2004).
5. M. Bedewy, E.R. Meshot, H. Guo, E.A. Verploegen, W. Lu, and A.J. Hart: Collective mechanism for the evolution and self-termination of vertically aligned carbon nanotube growth. *J. Phys. Chem. C* **113**(48), 20576 (2009).
6. E. Meshot, M. Bedewy, K. Lyons, A. Woll, K. Juggernauth, S. Tawfick, and A. Hart: Measuring the lengthening kinetics of aligned nanostructures by spatiotemporal correlation of height and orientation. *Nanoscale* **2**(6), 896 (2010).
7. M. Bedewy, E.R. Meshot, M.J. Reinker, and A.J. Hart: Population growth dynamics of carbon nanotubes. *ACS Nano* **5**(11), 8974 (2011).
8. M. Bedewy, E.R. Meshot, and A.J. Hart: Diameter-dependent kinetics of activation and deactivation in carbon nanotube population growth. *Carbon* **50**(14), 5106 (2012).
9. A.A. Puretzky, D.B. Geohegan, S. Jesse, I.N. Ivanov, and G. Eres: *In situ* measurements and modeling of carbon nanotube array growth kinetics during chemical vapor deposition. *Appl. Phys. A: Mater. Sci. Process.* **81**(2), 223 (2005).
10. D.N. Futaba, K. Hata, T. Namai, T. Yamada, K. Mizuno, Y. Hayamizu, M. Yumura, and S. Iijima: 84% catalyst activity of water-assisted growth of single walled carbon nanotube forest characterization by a statistical and macroscopic approach. *J. Phys. Chem. B* **110**(15), 8035 (2006).
11. S. Noda, K. Hasegawa, H. Sugime, K. Kakehi, Z. Zhang, S. Maruyama, and Y. Yukio: Millimeter-thick single-walled carbon nanotube forests: Hidden role of catalyst support. *Jpn. J. Appl. Phys.* **46**(5L), L399 (2007).
12. E. Einarsson, Y. Murakami, M. Kadowaki, and S. Maruyama: Growth dynamics of vertically aligned single-walled carbon nanotubes from *in situ* measurements. *Carbon* **46**(6), 923 (2008).
13. C.T. Wirth, C. Zhang, G. Zhong, S. Hofmann, and J. Robertson: Diffusion- and reaction-limited growth of carbon nanotube forests. *ACS Nano* **3**(11), 3560 (2009).
14. P. Vinten, J. Lefebvre, and P. Finnie: Kinetic critical temperature and optimized chemical vapor deposition growth of carbon nanotubes. *Chem. Phys. Lett.* **469**(4–6), 293 (2009).
15. P.B. Amama, C.L. Pint, S.M. Kim, L. McJilton, K.G. Eyink, E.A. Stach, R.H. Hauge, and B. Maruyama: Influence of alumina type on the evolution and activity of alumina-supported Fe catalysts in single-walled carbon nanotube carpet growth. *ACS Nano* **4**(2), 895 (2010).
16. P.B. Amama, C.L. Pint, L. McJilton, S.M. Kim, E.A. Stach, P.T. Murray, R.H. Hauge, and B. Maruyama: Role of water in super growth of single-walled carbon nanotube carpets. *Nano Lett.* **9**(1), 44 (2009).
17. S. Pathak, N. Mohan, E. Decolvenaere, A. Needleman, M. Bedewy, A.J. Hart, and J.R. Greer: Local relative density modulates failure and strength in vertically aligned carbon nanotubes. *ACS Nano* **7**(10), 8593 (2013).
18. M. Bedewy and A.J. Hart: Mechanical coupling limits the density and quality of self-organized carbon nanotube growth. *Nanoscale* **5**(7), 2928 (2013).
19. C.V. Thompson: Solid-state dewetting of thin films. *Annu. Rev. Mater. Res.* **42**, 399 (2012).
20. K.B.K. Teo, M. Chhowalla, G.A.J. Amaratunga, W.I. Milne, D.G. Hasko, G. Pirio, P. Legagneux, F. Wyczisk, and D. Pribat: Uniform patterned growth of carbon nanotubes without surface carbon. *Appl. Phys. Lett.* **79**(10), 1534 (2001).
21. Y. Li, J. Liu, Y. Wang, and Z.L. Wang: Preparation of monodispersed Fe−Mo nanoparticles as the catalyst for CVD synthesis of carbon nanotubes. *Chem. Mater.* **13**(3), 1008 (2001).
22. E.S. Polsen, M. Bedewy, and A.J. Hart: Decoupled control of carbon nanotube forest density and diameter by continuous-feed convective assembly of catalyst particles. *Small* **9**(15), 2564 (2013).
23. C. Hinderling, Y. Keles, T. Stöckli, H.F. Knapp, T. de los Arcos, P. Oelhafen, I. Korczagin, M.A. Hempenius, G.J. Vancso, R. Pugin, and H. Heinzelmann: Organometallic block copolymers as catalyst precursors for templated carbon nanotube growth. *Adv. Mater.* **16**(11), 876 (2004).
24. R.T.K. Baker, M.A. Barber, P.S. Harris, F.S. Feates, and R.J. Waite: Nucleation and growth of carbon deposits from the nickel catalyzed decomposition of acetylene. *J. Catal.* **26**(1), 51 (1972).
25. A.R. Harutyunyan, O.A. Kuznetsov, C.J. Brooks, E. Mora, and G. Chen: Thermodynamics behind carbon nanotube growth via endothermic catalytic decomposition reaction. *ACS Nano* **3**(2), 379 (2009).
26. S.M. Bachilo, L. Balzano, J.E. Herrera, F. Pompeo, D.E. Resasco, and R.B. Weisman: Narrow (n,m)-distribution of single-walled carbon nanotubes grown using a solid supported catalyst. *J. Am. Chem. Soc.* **125**(37), 11186 (2003).
27. T. de los Arcos, M. Gunnar Garnier, P. Oelhafen, D. Mathys, J. Won Seo, C. Domingo, J. Vicente García-Ramos, and S. Sánchez-Cortés: Strong influence of buffer layer type on carbon nanotube characteristics. *Carbon* **42**(1), 187 (2004).
28. W-H. Chiang and R.M. Sankaran: Synergistic effects in bimetallic nanoparticles for low temperature carbon nanotube growth. *Adv. Mater.* **20**(24), 4857 (2008).
29. B. Kitiyanan, W.E. Alvarez, J.H. Harwell, and D.E. Resasco: Controlled production of single-wall carbon nanotubes by catalytic decomposition of CO on bimetallic Co–Mo catalysts. *Chem. Phys. Lett.* **317**(3–5), 497 (2000).
30. S. Wang, A.Y. Borisevich, S.N. Rashkeev, M.V. Glazoff, K. Sohlberg, S.J. Pennycook, and S.T. Pantelides: Dopants adsorbed as single atoms prevent degradation of catalysts. *Nat. Mater.* **3**(3), 143 (2004).
31. V. Shanov, A. Gorton, Y.H. Yun, and M. Schulz: Composite catalyst and method for manufacturing carbon nanostructured materials, US Patent Application 2008/095695.
32. A.E. Islam, P. Nikolaev, P.B. Amama, S. Saber, D. Zakharov, D. Huffman, M. Erford, G. Sargent, S.L. Semiatin, E.A. Stach, and B. Maruyama: Engineering the activity and lifetime of heterogeneous catalysts for carbon nanotube growth via substrate ion beam bombardment. *Nano Lett.* **14**(9), 4997 (2014).
33. H. Dai, A.G. Rinzler, P. Nikolaev, A. Thess, D.T. Colbert, and R.E. Smalley: Single-wall nanotubes produced by metal-catalyzed disproportionation of carbon monoxide. *Chem. Phys. Lett.* **260**(3), 471 (1996).
34. I. Sushumna and E. Ruckenstein: Role of physical and chemical interactions in the behavior of supported metal-catalysts—iron on alumina—A case-study. *J. Catal.* **94**(1), 239 (1985).
35. A. Gohier, C.P. Ewels, T.M. Minea, and M.A. Djouadi: Carbon nanotube growth mechanism switches from tip- to base-growth with decreasing catalyst particle size. *Carbon* **46**(10), 1331 (2008).
36. M. Stadermann, S.P. Sherlock, J-B. In, F. Fornasiero, H.G. Park, A.B. Artyukhin, Y. Wang, J.J. De Yoreo, C.P. Grigoropoulos, O. Bakajin, A.A. Chernov, and A. Noy: Mechanism and kinetics of growth termination in controlled chemical vapor deposition growth of multiwall carbon nanotube arrays. *Nano Lett.* **9**(2), 738 (2009).
37. K. Hasegawa and S. Noda: Diameter increase in millimeter-tall vertically aligned single-walled carbon nanotubes during growth. *Appl. Phys. Express* **3**(4), 045103 (2010).

38. E.R. Meshot, E. Verploegen, M. Bedewy, S. Tawfick, A.R. Woll, K.S. Green, M. Hromalik, L.J. Koerner, H.T. Philipp, M.W. Tate, S.M. Gruner, and A.J. Hart: High-speed *in situ* X-ray scattering of carbon nanotube film nucleation and self-organization. *ACS Nano* **6**(6), 5091 (2012).
39. T. de los Arcos, M.G. Garnier, J.W. Seo, P. Oelhafen, V. Thommen, and D. Mathys: The influence of catalyst chemical state and morphology on carbon nanotube growth. *J. Phys. Chem. B* **108**(23), 7728 (2004).
40. C. Mattevi, C.T. Wirth, S. Hofmann, R. Blume, M. Cantoro, C. Ducati, C. Cepek, A. Knop-Gericke, S. Milne, C. Castellarin-Cudia, S. Dolafi, A. Goldoni, R. Schloegl, and J. Robertson: *In-situ* X-ray photoelectron spectroscopy study of catalyst−support interactions and growth of carbon nanotube forests. *J. Phys. Chem. C* **112**(32), 12207 (2008).
41. S. Hofmann, R. Sharma, C. Ducati, G. Du, C. Mattevi, C. Cepek, M. Cantoro, S. Pisana, A. Parvez, F. Cervantes-Sodi, A.C. Ferrari, R. Dunin-Borkowski, S. Lizzit, L. Petaccia, A. Goldoni, and J. Robertson: *In situ* observations of catalyst dynamics during surface-bound carbon nanotube nucleation. *Nano Lett.* **7**(3), 602 (2007).
42. S. Hofmann, R. Blume, C.T. Wirth, M. Cantoro, R. Sharma, C. Ducati, M. Hävecker, S. Zafeiratos, P. Schnoerch, A. Oestereich, D. Teschner, M. Albrecht, A. Knop-Gericke, R. Schlögl, and J. Robertson: State of transition metal catalysts during carbon nanotube growth. *J. Phys. Chem. C* **113**(5), 1648 (2009).
43. M. Bedewy, B. Viswanath, E.R. Meshot, D.N. Zakharov, E.A. Stach, and A.J. Hart: Measurement of the dewetting, nucleation, and deactivation kinetics of carbon nanotube population growth by environmental transmission electron microscopy. *Chem. Mater.* **28**(11), 3804 (2016).
44. R. Sharma, E. Moore, P. Rez, and M.M.J. Treacy: Site-specific fabrication of Fe particles for carbon nanotube growth. *Nano Lett.* **9**(2), 689 (2009).
45. Y-Q. Xu, E. Flor, H. Schmidt, R.E. Smalley, and R.H. Hauge: Effects of atomic hydrogen and active carbon species in 1 mm vertically aligned single-walled carbon nanotube growth. *Appl. Phys. Lett.* **89**(12), 123116 (2006).
46. C.L. Pint, S.M. Kim, E.A. Stach, and R.H. Hauge: Rapid and scalable reduction of dense surface-supported metal-oxide catalyst with hydrazine vapor. *ACS Nano* **3**(7), 1897 (2009).
47. P. Landois, M. Pinault, S. Rouzière, D. Porterat, C. Mocuta, E. Elkaim, M. Mayne-L'Hermite, and P. Launois: *In situ* time resolved wide angle X-ray diffraction study of nanotube carpet growth: Nature of catalyst particles and progressive nanotube alignment. *Carbon* **87**, 246 (2015).
48. J-P. Tessonnier and D.S. Su: Recent progress on the growth mechanism of carbon nanotubes: A review. *ChemSusChem* **4**(7), 824 (2011).
49. S. Mazzucco, Y. Wang, M. Tanase, M. Picher, K. Li, Z. Wu, S. Irle, and R. Sharma: Direct evidence of active and inactive phases of Fe catalyst nanoparticles for carbon nanotube formation. *J. Catal.* **319**, 54 (2014).
50. C.T. Wirth, B.C. Bayer, A.D. Gamalski, S. Esconjauregui, R.S. Weatherup, C. Ducati, C. Baehtz, J. Robertson, and S. Hofmann: The phase of iron catalyst nanoparticles during carbon nanotube growth. *Chem. Mater.* **24**(24), 4633 (2012).
51. M. Lin, J.P.Y. Tan, C. Boothroyd, K.P. Loh, E.S. Tok, and Y.L. Foo: Direct observation of single-walled carbon nanotube growth at the atomistic scale. *Nano Lett.* **6**(3), 449 (2006).
52. H. Yoshida, S. Takeda, T. Uchiyama, H. Kohno, and Y. Homma: Atomic-scale *in situ* observation of carbon nanotube growth from solid state iron carbide nanoparticles. *Nano Lett.* **8**(7), 2082 (2008).
53. M. Moseler, F. Cervantes-Sodi, S. Hofmann, G. Csanyi, and A.C. Ferrari: Dynamic catalyst restructuring during carbon nanotube growth. *ACS Nano* **4**(12), 7587 (2010).
54. V. Balakrishnan, M. Bedewy, E.R. Meshot, S.W. Pattinson, E.S. Polsen, F. Laye, D.N. Zakharov, E.A. Stach, and A.J. Hart: Real time imaging of self-organization and mechanical competition in carbon nanotube forest growth. *ACS Nano* (2017). Accepted.
55. Z.P. Huang, J.W. Xu, Z.F. Ren, J.H. Wang, M.P. Siegal, and P.N. Provencio: Growth of highly oriented carbon nanotubes by plasma-enhanced hot filament chemical vapor deposition. *Appl. Phys. Lett.* **73**(26), 3845 (1998).
56. S. Fan, M.G. Chapline, N.R. Franklin, T.W. Tombler, A.M. Cassell, and H. Dai: Self-oriented regular arrays of carbon nanotubes and their field emission properties. *Science* **283**(5401), 512 (1999).
57. J. Kong, A.M. Cassell, and H. Dai: Chemical vapor deposition of methane for single-walled carbon nanotubes. *Chem. Phys. Lett.* **292**(4–6), 567 (1998).
58. S. Maruyama, E. Einarsson, Y. Murakami, and T. Edamura: Growth process of vertically aligned single-walled carbon nanotubes. *Chem. Phys. Lett.* **403**(4–6), 320 (2005).
59. B. Zheng, C. Lu, G. Gu, A. Makarovski, G. Finkelstein, and J. Liu: Efficient CVD growth of single-walled carbon nanotubes on surfaces using carbon monoxide precursor. *Nano Lett.* **2**(8), 895 (2002).
60. Y. Zhang, J.M. Gregoire, R.B. van Dover, and A.J. Hart: Ethanol-promoted high-yield growth of few-walled carbon nanotubes. *J. Phys. Chem. C* **114**(14), 6389 (2010).
61. D.N. Futaba, J. Goto, S. Yasuda, T. Yamada, M. Yumura, and K. Hata: General rules governing the highly efficient growth of carbon nanotubes. *Adv. Mater.* **21**(47), 4811 (2009).
62. C.L. Pint, S.T. Pheasant, A.N.G. Parra-Vasquez, C. Horton, Y. Xu, and R.H. Hauge: Investigation of optimal parameters for oxide-assisted growth of vertically aligned single-walled carbon nanotubes. *J. Phys. Chem. C* **113**(10), 4125 (2009).
63. X. Li, X. Zhang, L. Ci, R. Shah, C. Wolfe, S. Kar, S. Talapatra, and P. Ajayan: Air-assisted growth of ultra-long carbon nanotube bundles. *Nanotechnology* **19**(45), 455609 (2008).
64. L. Zhu, D.W. Hess, and C-P. Wong: Monitoring carbon nanotube growth by formation of nanotube stacks and investigation of the diffusion-controlled kinetics. *J. Phys. Chem. B* **110**(11), 5445 (2006).
65. P. Vinten, P. Marshall, J. Lefebvre, and P. Finnie: Distinct termination morphologies for vertically aligned carbon nanotube forests. *Nanotechnology* **21**(3), 035603 (2010).
66. V. Meunier and P. Lambin: Scanning tunneling microscopy and spectroscopy of topological defects in carbon nanotubes. *Carbon* **38**(11–12), 1729 (2000).
67. A.J. Hart, L. van Laake, and A.H. Slocum: Desktop growth of carbon-nanotube monoliths with *in situ* optical imaging. *Small* **3**(5), 772 (2007).
68. A.A. Puretzky, G. Eres, C.M. Rouleau, I.N. Ivanov, and D.B. Geohegan: Real-time imaging of vertically aligned carbon nanotube array growth kinetics. *Nanotechnology* **19**(5), 055605 (2008).
69. D-H. Kim, H-S. Jang, C-D. Kim, D-S. Cho, H-S. Yang, H-D. Kang, B-K. Min, and H-R. Lee: Dynamic growth rate behavior of a carbon nanotube forest characterized by *in situ* optical growth monitoring. *Nano Lett.* **3**(6), 863 (2003).
70. L.M. Dell'Acqua-Bellavitis, J.D. Ballard, P.M. Ajayan, and R.W. Siegel: Kinetics for the synthesis reaction of aligned carbon nanotubes: A study based on *in situ* diffractography. *Nano Lett.* **4**(9), 1613 (2004).

71. E.R. Meshot and A.J. Hart: Abrupt self-termination of vertically aligned carbon nanotube growth. *Appl. Phys. Lett.* **92**(11), 113107 (2008).
72. E.R. Meshot, D.L. Plata, S. Tawfick, Y. Zhang, E.A. Verploegen, and A.J. Hart: Engineering vertically aligned carbon nanotube growth by decoupled thermal treatment of precursor and catalyst. *ACS Nano* **3**(9), 2477 (2009).
73. T. Iwasaki, G.F. Zhong, T. Aikawa, T. Yoshida, and H. Kawarada: Direct evidence for root growth of vertically aligned single-walled carbon nanotubes by microwave plasma chemical vapor deposition. *J. Phys. Chem. B* **109**(42), 19556 (2005).
74. S.P. Patole, J.H. Park, T.Y. Lee, J.H. Lee, A.S. Patole, and J.B. Yoo: Growth interruption studies on vertically aligned 2-3 wall carbon nanotubes by water assisted chemical vapor deposition. *Appl. Phys. Lett.* **93**(11), 114101 (2008).
75. S. Yasuda, T. Hiraoka, D.N. Futaba, T. Yamada, M. Yumura, and K. Hata: Existence and kinetics of graphitic carbonaceous impurities in carbon nanotube forests to assess the absolute purity. *Nano Lett.* **9**(2), 769 (2009).
76. A.M. Valiente, P.N. Lopez, I.R. Ramos, A.G. Ruiz, C. Li, and Q. Xin: *In situ* study of carbon nanotube formation by $C_2H_2$ decomposition on an iron-based catalyst. *Carbon* **38**(14), 2003 (2000).
77. J.J. Jackson, A.A. Puretzky, K.L. More, C.M. Rouleau, G. Eres, and D.B. Geohegan: Pulsed growth of vertically aligned nanotube arrays with variable density. *ACS Nano* **4**(12), 7573 (2010).
78. D.B. Geohegan, A.A. Puretzky, J.J. Jackson, C.M. Rouleau, G. Eres, and K.L. More: Flux-dependent growth kinetics and diameter selectivity in single-wall carbon nanotube arrays. *ACS Nano* **5**(10), 8311 (2011).
79. A.A. Puretzky, D.B. Geohegan, J.J. Jackson, S. Pannala, G. Eres, C.M. Rouleau, K.L. More, N. Thonnard, and J.D. Readle: Incremental growth of short SWNT arrays by pulsed chemical vapor deposition. *Small* **8**(10), 1534 (2012).
80. M. Picher, E. Anglaret, R. Arenal, and V. Jourdain: Self-deactivation of single-walled carbon nanotube growth studied by *in situ* Raman measurements. *Nano Lett.* **9**(2), 542 (2009).
81. S. Chiashi, M. Kohno, Y. Takata, and S. Maruyama: Localized synthesis of single-walled carbon nanotubes on silicon substrates by a laser heating catalytic CVD. *J. Phys. Conf. Ser.* **59**, 155–158 (2007).
82. A. Li-Pook-Than, J. Lefebvre, and P. Finnie: Phases of carbon nanotube growth and population evolution from *in situ* Raman spectroscopy during chemical vapor deposition. *J. Phys. Chem. C* **114**(25), 11018 (2010).
83. N. Latorre, E. Romeo, F. Cazana, T. Ubieto, C. Royo, J.J. Villacampa, and A. Monzon: Carbon nanotube growth by catalytic chemical vapor deposition: A phenomenological kinetic model. *J. Phys. Chem. C* **114**(11), 4773 (2010).
84. R. Rao, D. Liptak, T. Cherukuri, B.I. Yakobson, and B. Maruyama: *In situ* evidence for chirality-dependent growth rates of individual carbon nanotubes. *Nat. Mater.* **11**(3), 213 (2012).
85. B.N. Wang, R.D. Bennett, E. Verploegen, A.J. Hart, and R.E. Cohen: Quantitative characterization of the morphology of multiwall carbon nanotube films by small-angle X-ray scattering. *J. Phys. Chem. C* **111**(16), 5859 (2007).
86. H. Wang, Z. Xu, and G. Eres: Order in vertically aligned carbon nanotube arrays. *Appl. Phys. Lett.* **88**(21), 213111 (2006).
87. O.A. Louchev, T. Laude, Y. Sato, and H. Kanda: Diffusion-controlled kinetics of carbon nanotube forest growth by chemical vapor deposition. *J. Chem. Phys.* **118**(16), 7622 (2003).
88. R.F. Wood, S. Pannala, J.C. Wells, A.A. Puretzky, and D.B. Geohegan: Simple model of the interrelation between single- and multiwall carbon nanotube growth rates for the CVD process. *Phys. Rev. B: Condens. Matter Mater. Phys.* **75**(23), 235446 (2007).
89. B.N. Wang, R.D. Bennett, E. Verploegen, A.J. Hart, and R.E. Cohen: Characterizing the morphologies of mechanically manipulated multiwall carbon nanotube films by small-angle X-ray scattering. *J. Phys. Chem. C* **111**(48), 17933 (2007).
90. E. Verploegen, A.J. Hart, M. De Volder, S. Tawfick, K-K. Chia, and R.E. Cohen: Non-destructive characterization of structural hierarchy within aligned carbon nanotube assemblies. *J. Appl. Phys.* **109**(9), 094316 (2011).
91. C.L. Pint, Y-Q. Xu, M. Pasquali, and R.H. Hauge: Formation of highly dense aligned ribbons and transparent films of single-walled carbon nanotubes directly from carpets. *ACS Nano* **2**(9), 1871 (2008).
92. G. Zhong, J.H. Warner, M. Fouquet, A.W. Robertson, B. Chen, and J. Robertson: Growth of ultrahigh density single-walled carbon nanotube forests by improved catalyst design. *ACS Nano* **6**(4), 2893 (2012).
93. S.K. Youn, N. Yazdani, J. Patscheider, and H.G. Park: Facile diameter control of vertically aligned, narrow single-walled carbon nanotubes. *RSC Adv.* **3**(5), 1434 (2013).
94. J.R. Sanchez-Valencia, T. Dienel, O. Groning, I. Shorubalko, A. Mueller, M. Jansen, K. Amsharov, P. Ruffieux, and R. Fasel: Controlled synthesis of single-chirality carbon nanotubes. *Nature* **512**(7512), 61 (2014).
95. S. Esconjauregui, B.C. Bayer, M. Fouquet, C.T. Wirth, C. Ducati, S. Hofmann, and J. Robertson: Growth of high-density vertically aligned arrays of carbon nanotubes by plasma-assisted catalyst pretreatment. *Appl. Phys. Lett.* **95**(17), 173115 (2009).
96. M. Bedewy, B. Farmer, and A.J. Hart: Synergetic chemical coupling controls the uniformity of carbon nanotube microstructure growth. *ACS Nano* **8**(6), 5799 (2014).
97. M. De Volder, S. Park, S. Tawfick, and A.J. Hart: Strain-engineered manufacturing of freeform carbon nanotube microstructures. *Nat. Commun.* **5**, 4512 (2014).
98. D.N. Futaba, K. Hata, T. Yamada, K. Mizuno, M. Yumura, and S. Iijima: Kinetics of water-assisted single-walled carbon nanotube synthesis revealed by a time-evolution analysis. *Phys. Rev. Lett.* **95**(5), 056104 (2005).
99. A.I. La Cava, C.A. Bernardo, and D.L. Trimm: Studies of deactivation of metals by carbon deposition. *Carbon* **20**(3), 219 (1982).
100. S.M. Kim, C.L. Pint, P.B. Amama, D.N. Zakharov, R.H. Hauge, B. Maruyama, and E.A. Stach: Evolution in catalyst morphology leads to carbon nanotube growth termination. *J. Phys. Chem. Lett.* **1**(6), 918 (2010).
101. R.G. de Villoria, S.L. Figueredo, A.J. Hart, S.A. Steiner, A.H. Slocum, and B.L. Wardle: High-yield growth of vertically aligned carbon nanotubes on a continuously moving substrate. *Nanotechnology* **20**(40), 405611 (2009).
102. S.N. Yoshikawa, T. Asari, N. Kishi, S. Hayashi, T. Sugai, and H. Shinohara: An efficient fabrication of vertically aligned carbon nanotubes on flexible aluminum foils by catalyst-supported chemical vapor deposition. *Nanotechnology* **19**(24), 245607 (2008).
103. Y. Zhou, L. Hu, and G. Grüner: A method of printing carbon nanotube thin films. *Appl. Phys. Lett.* **88**(12), 123109 (2006).
104. L. Ge, S. Sethi, L. Ci, P.M. Ajayan, and A. Dhinojwala: Carbon nanotube-based synthetic gecko tapes. *Proc. Natl. Acad. Sci.* **104** (26), 10792 (2007).
105. S. Tawfick, K. O'Brien, and A.J. Hart: Flexible high-conductivity carbon-nanotube interconnects made by rolling and printing. *Small* **5**(21), 2467 (2009).